Catalysis Science & Technology

Accepted Manuscript

ROYAL SOCIETY OF CHEMISTRY

www.rsc.org/catalysis

TOC

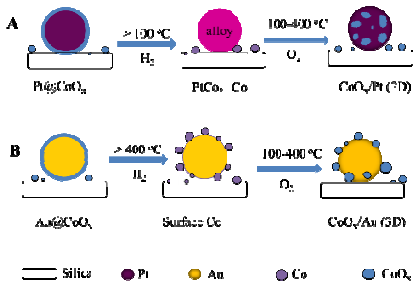

Active CoO_x-on-Pt structure was prepared differently in comparison with CoO_x-on-Au structure due to the different interaction of Co (CoO_x) with Pt and Au.

Catalysis
Science & Technology

RSCPublishing

PAPER

Comparative studies in redox behaviors of Pt-Co/SiO_2 and Au-Co/SiO_2 catalysts and their activities in CO oxidation

Cite this: DOI: 10.1039/x0xx00000x

Xuejun Xu[a], Qiang Fu*[a], Mingming Wei[a], Xing Wu[b], and Xinhe Bao[a]

Received ooth Marth 2014,
Accepted ooth Marth 2014

DOI: 10.1039/x0xx00000x

www.rsc.org/

Silica supported Pt-Co and Au-Co nanoparticles (NPs) were treated by various redox processes and characterized by X-ray diffraction, X-ray absorption near edge structure, and X-ray photoelectron spectroscopy. We found that most of Co oxide (CoO_x) species on Pt NPs can be reduced within 100 ^oC and form alloy structure with Pt at elevated temperatures. Oxidation of Co in the reduced sample takes place gradually with increasing temperatures. In contrast, temperatures higher than 400 ^oC are needed to reduce CoO_x on Au NPs and Co atoms hardly form alloy with Au even at 600 ^oC. The Co species in the reduced Au-Co/SiO_2 sample were quickly oxidized in O_2 atmosphere at room temperature. High CO oxidation activity was observed in the Pt-Co/SiO_2 catalysts reduced below 300 ^oC, but this necessitates a reduction at 600 ^oC for the Au-Co/SiO_2 catalysts. All the results illustrate a stronger interaction of Co (CoO_x) with Pt than Au. In both systems, the optimum treatment condition is to produce the similar CoO-on-noble metal (NM) active structure and maximize the density of interface sites between surface CoO structure and NM support.

Introduction

Co-based catalysts have been used in many important energy-related processes. For example, supported Co nanoparticles (NPs) are considered as one of the most promising catalysts for Fischer–Tropsch (FT) processes.[1] The catalytic activity and stability are strongly dependent on the reducibility and dispersion of Co NPs.[2-5] Noble metals (NMs) including Pt, Re, Ru and Au were often added to the Co catalysts to enhance their overall catalytic performance.[6-10] Co oxides (CoO_x) exhibit excellent catalytic performances in CO oxidation at low temperatures[11-13] and oxygen reduction reaction (ORR)/oxygen evolution reaction (OER).[14-16] It has been found that the combination with NMs can further increase their performances. For instance, catalysts consisting of Co_3O_4 and Au NPs can catalyze CO oxidation at temperatures below 0 ^oC.[17] Pt NPs decorated with CoO_x are highly active for CO oxidation in excess of H_2, which completely remove CO from H_2 at room temperature.[18, 19] In OER reactions, the activity of 0.4 monolayer (ML) CoO_x deposited on Au surface is ~40 times higher than the pure Co oxides.[20] The synergetic effect between the two components is attributed to the improved performance, which is strongly dependent on the interaction between NM and Co (CoO_x). The NM-Co interaction is of great importance for the FT and hydrogenation reactions, and the interaction between NM and CoO_x is critical for these O_2-containing reactions such as CO oxidation and ORR. Thus, understanding the nature of the NM-Co (CoO_x) interaction is highly important for the Co-catalyzed reactions.

In the present work, we made a comparative study in the reduction and oxidation behaviors of Pt-Co/SiO_2 and Au-Co/SiO_2 bi-component catalysts as well as their activity in the CO oxidation reactions. Our results show that Pt exhibits a much stronger effect on the redox process of Co (CoO_x) than Au due to the stronger interaction of Co (CoO_x) with Pt. The different interaction between NMs and transition metal (TMs) or TM oxides should be considered for rational design of bimetallic catalysts and oxide/NM inverse catalysts.[21-25]

Experimental section

Pt-Co/SiO_2 and Au-Co/SiO_2 catalysts were prepared using a two-step synthetic method, similar to that for the preparation of Pt-Fe/SiO_2 catalysts.[26] Briefly, 1 g commercial silica (Qingdao Ocean Chemical Company) was functionalized with APTES ($H_2N(CH_2)_3Si(OEt)_3$). Then, 8.4 ml $HAuCl_4$ solution (2.5×10^{-2} mol/L) was added to the functionalized SiO_2 support, followed by reduction with $NaBH_4$ (6.3×10^{-1} mol/L). After filtration and washing, 4.1 mL $Co(NO_3)_2$ solution (5.0×10^{-2} mol/L) was added to the resulted Au/SiO_2 powders and reduced onto the Au NPs surfaces using hydrazine hydrate at 75 ^oC.[27] The Pt-Co/SiO_2 catalysts were also prepared by a similar process, in which 10.6 mL H_2PtCl_6 solution (1.9×10^{-2} mol/L) was firstly reduced onto the functionalized SiO_2 support by $NaBH_4$. In the subsequent step, 4.1 mL $Co(NO_3)_2$ solution (5.0×10^{-2} mol/L) was added and reduced using hydrazine hydrate at 50 ^oC. The nominal loading of Au and Pt is fixed at 4%, and the atomic ratio of Au (Pt) and Co is about 1/1.

The as-prepared Pt-Co/SiO_2 and Au-Co/SiO_2 samples were calcined at 400 ^oC in air in a muffle furnace. Then, the calcined samples were treated in O_2 or H_2 gas with a flow rate of 30 ml/min and heated at a specific temperature for 2 h. After cooling down to room temperature, the gas stream was switched to the reaction atmosphere, i.e., CO oxidation in excess O_2 (COOX): 1% CO and 20% O_2 balanced with He, or CO oxidation in stoichiometric O_2: 1%

CO and 0.5% O_2 balanced with He, with a flow rate of 50 ml/min. The gas hourly space velocity (GHSV) is equal to 75000 ml·g^{-1}·h^{-1}, if not specified. The catalytic performance was investigated from 30 °C to 200 °C (Pt-Co/SiO_2) or 300 °C (Au-Co/SiO_2) with the heating rate of 1 °C/min. Gas products were analyzed by a micro gas chromatograph (Agilent Micro GC-490) equipped with a 5 Å molecular sieve column and a thermal conductivity detector.

X-ray diffraction (XRD) patterns were collected on a Rigaku D/Max 2500 diffractometer using a Cu Kα (λ = 1.5406 Å) radiation source. Transmission electron microscopy (TEM) studies were carried out on FEI Tecnai G2 microscope operated at an acceleration voltage of 120 kV and JEM-2100F equipped with oxford EDS X-Max80 (HR-TEM). X-ray photoelectron spectroscopy (XPS) measurements were performed using Thermo Scientific ESCALAB 250Xi spectrometer. The XP spectra were obtained with an Al Kα X-ray source, and the passing energy was fixed at 20 eV. The Si 2p peak located at 103.9 eV from the SiO_2 support was used for calibration of binding energies. The total metal loadings were determined by leaching the samples in an aqua regia solution, and the metal ion concentrations in the leached solutions were measured by inductively coupled plasma atomic emission spectrometry (ICP-AES) (ICPS-8100, Shimadzu). Co species outside of NM particles were selectively leached in a dilute nitric acid solution (5.0×10^{-2} mol/L) and the Co contents were also determined by ICP-AES. X-ray absorption near edge structure (XANES) was measured at the BL14W1 beamline of the Shanghai Synchrotron Radiation Facility (SSRF). In-situ Co K-edge XANES spectra of the catalysts were collected in fluorescence mode. For comparison, those of Co foil and standard CoO and Co_3O_4 sample were recorded in transmission mode.

Results

The as-prepared Pt-Co/SiO_2 and Au-Co/SiO_2 samples were calcined at 400 °C in air to remove the organic groups on the silica surfaces. ICP-AES results show that the actual loadings of Au and Pt are ca. 4.6% and 4.5%, and the atomic ratios of Au/Co and Pt/Co are 1.09/1 and 1.07/1, respectively (Table S1). The calcined samples were then subjected to further reduction and/or oxidation treatments. Firstly, XRD was applied to investigate the structural changes of the Pt-Co/SiO_2 and Au-Co/SiO_2 samples, which were either reduced in H_2 or oxidized in O_2 at various temperatures. For the as-calcined Pt-Co/SiO_2 samples, the diffraction peak of face-centered cubic (fcc) Pt(111) is located at 39.8°, which is the same as that of pure Pt NPs. The peak position slightly shifts to a higher angle upon reduction at 200 °C, and reaches to 40.3° after reduction at 600 °C (Figure 1A). The results indicate that Co species on Pt NPs can be reduced at low temperatures, which gradually diffuse into Pt NPs to form Pt_3Co alloys after reduction at 600 °C. Subsequently, the sample reduced at 600 °C was subjected to oxidation in O_2 between 100 and 400 °C. When exposed to the oxidative atmosphere, the Pt(111) diffraction peak shifts gradually to lower angles and changes back to its original position (39.8°) at 400 °C (Figure 2A). The present XRD data show that oxidation treatment can drive the outward diffusion of alloyed Co atoms from the cores of Pt NPs at elevated temperature.[18, 19, 28-30]

The XRD patterns acquired from the Au-Co/SiO_2 sample show that there is no significant change when reducing the sample in H_2 between 100 and 600 °C (Figure 1B). The formation of AuCo alloy has been shown to be difficult, which needs annealing at high temperatures e.g. 996.5 °C according to the Au-Co phase diagram.[31] Under the present reduction conditions, we infer that the inward diffusion of Co atoms into Au NPs has not occurred. It is also expected that the subsequent oxidation treatments of the reduced Au-Co/SiO_2 sample did not produce any change in the XRD patterns, and the main peak is still located at 38.2°, characteristic for the Au(111) peak (Figure 2B).

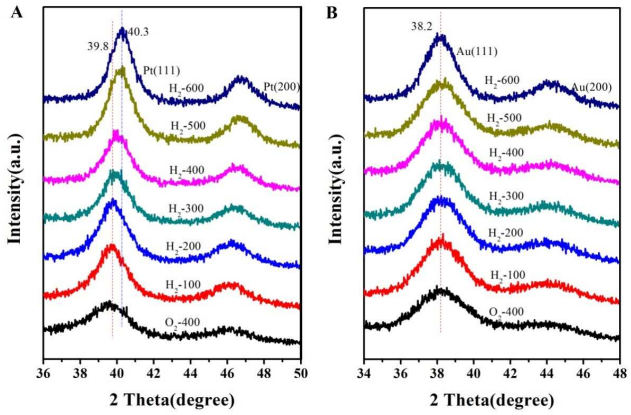

Figure 1. XRD patterns acquired from the as-calcined Pt-Co/SiO_2 (A) and Au-Co/SiO_2 (B) samples as well as these samples subjected to reduction in H_2 at different temperatures.

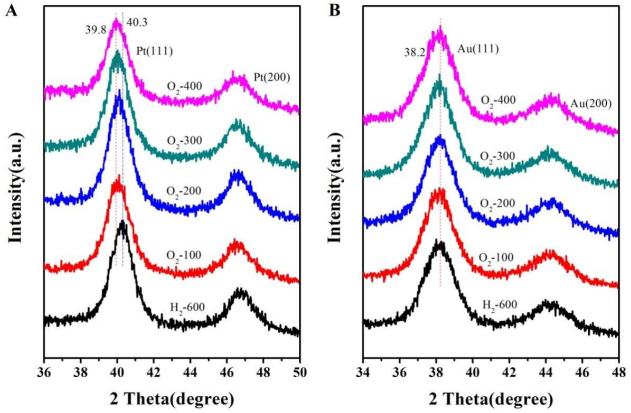

Figure 2. XRD patterns acquired from the reduced Pt-Co/SiO_2 (A) and Au-Co/SiO_2 (B) samples subjected to oxidation in O_2 at different temperatures.

TEM images show that as-prepared Pt and Au NPs are uniformly dispersed on SiO_2 surface, and average diameter of the Pt and Au NPs is 3.2 and 2.0 nm, respectively. With additional Co deposition, the formed Pt-Co and Au-Co NPs are little bigger, which have the sizes of 3.8 and 2.5 nm, respectively (Figure S1). After reduction at 600 °C, the particle sizes just increases slightly, reaching to 4.2 and 4.0 nm. For comparison, the average diameter of Pt and Au NPs reduced under the same condition is 3.5 and 5.8 nm (Figure S2). The addition of Co species can effectively prevent the sintering of Au NPs upon high temperature reduction while it has little influence on the sintering of Pt NPs (Figure 3a, 3b).

High resolution TEM (HR-TEM) images of the reduced Pt-Co/SiO_2 sample show that the d-spacing of (110) and (020) planes are ~2.92 and ~2.05 Å, respectively. The angle between the (110) and (020) planes is 46.57° (Figure 3c). The structural features are consistent with that of primitive cubic Pt_3Co alloy (JCPDS 29-0499). In the reduced Au-Co/SiO_2 catalyst, the d-spacing of the (111) and (200) planes are ~2.20 and ~2.00 Å, respectively. The angle between the (111) and (200) planes is 52.59° (Figure 3d), which is consistent with that of fcc Au

(JCPDS 04-0784). Thus, high temperature reduction did not produce any AuCo alloys.

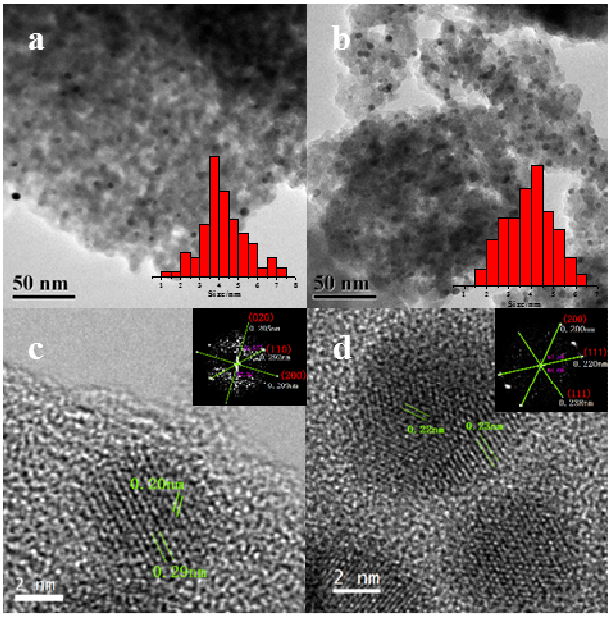

Figure 3. TEM and HR-TEM images from Pt-Co/SiO_2 and Au-Co/SiO_2 samples: a) and c), Pt-Co/SiO_2 reduced at 600 °C; b) and d), Au-Co/SiO_2 reduced at 600 °C; The size distribution of the NPs are shown in the insets of a) and b). The corresponding FFT analysis of the selected image is shown in the insets of c) and d).

Figures 4 and 5 show in-situ Co K-edge XANES spectra acquired from the Pt-Co/SiO_2 and Au-Co/SiO_2 samples treated in H_2 and O_2 environments at elevated temperature. For the as-calcined Pt-Co/SiO_2 and Au-Co/SiO_2 samples, the features of the absorption edge and white line peak resemble those of CoO, indicating that the cobalt species are resent as oxide (CoO_x), probably in the form of CoO.[32] Reduction of the as-calcined Pt-Co/SiO_2 sample in H_2 at 100 °C causes a big change in the Co K-edge spectrum. The absorption edge shifts to a lower energy position and the white line intensity decreases a lot, both of which are more like those of the Co foil (Figure 4A). With the reduction temperature increased from 100 to 600 °C, only slight change has been observed in the spectra. The results indicate that most of the CoO_x component in the Pt-Co/SiO_2 sample has been reduced within 100 °C. For the Au-Co/SiO_2 sample, the reduction at 100 °C only produces a small change in the Co K-edge spectrum (Figure 4B). Both the absorption edge and the white line peak gradually approach those of the Co foil with the increasing reduction temperatures. The Co K-edge of the sample reduced at 600 °C indicates the full reduction of the Co species. The results demonstrate that the presence of Au in the Au-Co/SiO_2 system did not facilitate the reduction of Co oxides significantly, in contrast with Pt-Co/SiO_2 system.

The reduced Pt-Co/SiO_2 and Au-Co/SiO_2 samples were undergoing oxidation treatments at various temperatures, which were also monitored by in-situ XANES. The main features of the Co K-edge spectra of the Pt-Co/SiO_2 sample show a gradual transition from the metallic Co to the oxidized Co when exposed to O_2 from room temperature to 400 °C (Figure 5A). However, the Co K-edge spectrum of the Au-Co/SiO_2 sample exposed to O_2 at room temperature already resembles that of CoO, and no big changes were observed when further oxidizing from 100 to 400 °C (Figure 5B). In the reduced Au-Co/SiO_2 sample, most of Co atoms are located outside of Au NPs and they can be fully oxidized upon exposure to O_2 at room temperature. In contrast, most of Co atoms are in the subsurface regions of Pt NPs in the reduced Pt-Co/SiO_2 sample.[18] Oxidation of the alloyed Co atoms can be kinetically limited at low temperatures, e.g. room temperature, and thus the full oxidation of Co species in the reduced Pt-Co/SiO_2 sample necessitates high temperatures.

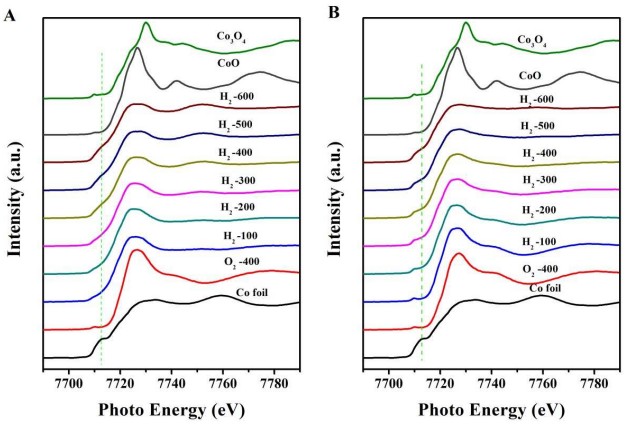

Figure 4. Co K-edge XANES spectra recorded from the as-calcined Pt-Co/SiO_2 (A) and Au-Co/SiO_2 (B) samples as well as these samples subjected to reduction in H_2 at different temperatures. The vertical lines show the positions of shoulder feature for Co foil, serving as a guide for tracing the absorption edge shift of Co upon redox treatments.

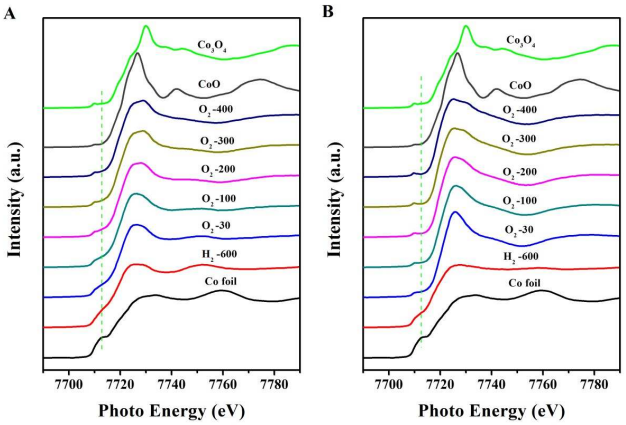

Figure 5. Co K-edge XANES spectra recorded from the reduced Pt-Co/SiO_2 (A) and Au-Co/SiO_2 (B) samples subjected to oxidation in O_2 at different temperatures.

Ex-situ XPS measurements were performed over the Pt-Co/SiO_2 and Au-Co/SiO_2 samples, which were treated under different redox conditions (Figures 6). The as-calcined Pt-Co/SiO_2 and Au-Co/SiO_2 samples present similar Co $2p_{3/2}$ spectra, both of which consist of a main peak at 782.1 eV and a strong satellite peak at 787.9 eV, and the $2p_{3/2}$-$2p_{1/2}$ spin-orbit splitting energy is 15.8 eV. It has been shown that the satellite peak at the high energy side of Co $2p_{3/2}$ is due to a shake-up process, which can be observed only in the high-spin Co^{2+} ion.[33, 34] Moreover, the $2p_{3/2}$-$2p_{1/2}$ spin-orbit splitting energy is an effective parameter to distinguish between CoO and Co_3O_4, which is 15.8 and 15.0 eV, respectively.[35] Thus, the XPS data suggest that the Co species in the as-calcined Pt-Co/SiO_2 and Au-Co/SiO_2 samples are mainly CoO, consistent with the XANES results.

Reduction treatment of the Pt-Co/SiO_2 sample at 600 °C leads to an appearance of a strong shoulder peak at 778.5 eV, which is from metallic Co. Our previous works have shown that the metallic

Co species are in the subsurface regions of Pt NPs and can resist oxidation under ambient conditions.[36-39] On the contrary, for the Au-Co/SiO_2 sample reduced at 600 °C there is only very small amount of metallic Co signal observed in the Co 2p spectrum.

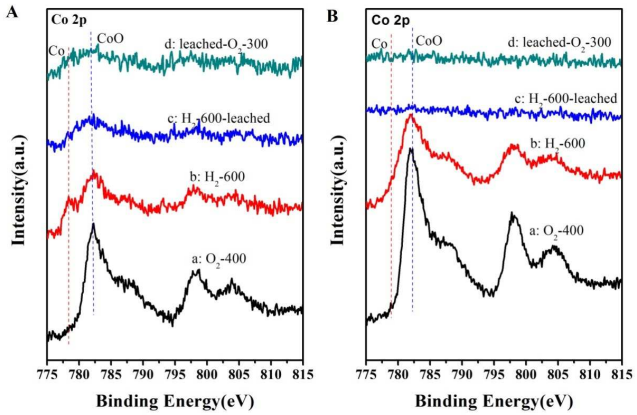

Figure 6. XPS Co 2p spectra from the Pt-Co/SiO_2 (A) and Au-Co/SiO_2 (B) samples subjected to different pretreatments: a) as-calcined at 400 °C; b) reduced at 600 °C; c) reduced samples leached by dilute nitric acid; d) leached samples subjected to oxidation at 300 °C;

To further investigate the alloying reaction between Co and NM, the reduced Pt-Co/SiO_2 and Au-Co/SiO_2 samples were leached by a dilute nitric acid solution. In this process, Co species on NM surfaces and outside of NM particles can be selectively removed, while those in the subsurface regions of the NM particles remain unaffected.[18] For reference, all the reduced samples were also washed with aqua regia solution in which all the Co species can be dissolved. The distribution of Co species can be determined by measuring Co ion concentrations of these leached solutions by ICP-AES. The data show that 64% Co species are leached out by the nitric acid solution and thus the residual 36% Co species are inside the Pt NPs forming Pt_3Co alloy. However, most of the Co species in the reduced Au-Co/SiO_2 sample are leached away by the nitric acid solution, indicating that there is little Co species alloyed with Au NPs (Table 1).

Table 1 The contents of Co species leached out from the Pt-Co/SiO_2 and Au-Co/SiO_2 samples reduced at 600 °C.

Sample	aqua regia/ppm	dilute nitric acid/ppm	Co leached out
Pt-Co/SiO_2	10.2254	6.5251	64%
Au-Co/SiO_2	10.1738	10.7348	100%

XPS Co 2p spectra of the leached samples show that there is no signal in the region of Co 2p for the leached Au-Co/SiO_2 sample and the sample oxidized at 300 °C (Figure 6). For the as-leached Pt-Co/SiO_2 sample, a considerable amount of Co and CoO species have been observed in the Co 2p spectrum. Upon oxidation at 300 °C, the metallic Co component gets weakened due to the oxidation-induced surface segregation of Co atoms at elevated temperatures.

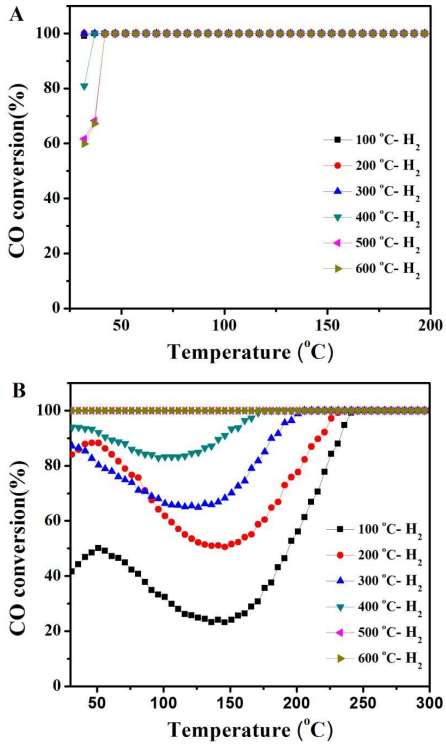

Figure 7. CO conversion light-off curves over the as-calcined Pt-Co/SiO_2 (A) and Au-Co/SiO_2 (B) samples reduced at different temperatures.

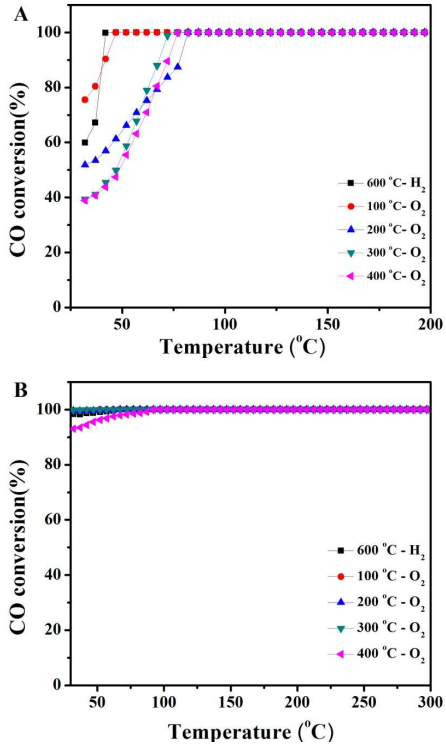

Figure 8. CO conversion light-off curves over the reduced Pt-Co/SiO_2 (A) and Au-Co/SiO_2 (B) samples oxidized at different temperatures.

COOX was chosen as a probe reaction to investigate the dependence of the activity of the Pt-Co/SiO_2 and Au-Co/SiO_2

catalysts on various treatments. For the Pt-Co/SiO_2 catalyst, remarkable activity has been obtained after the reduction treatment on the sample at 100 ^oC, and CO can be completely converted to CO_2 at room temperature. The catalyst reduced at 200 and 300 ^oC also exhibits a comparably high activity. Reduction above 400 ^oC, however, results in a slight decrease in the activity (Figure 7A). Figure 7B displays that the Au-Co/SiO_2 catalyst reduced at 100 ^oC shows much low activity and there is a dip valley in its light-off curve. The previous studies showed that a change in the reaction mechanism from the low temperature region to the high temperature region causes the specific reaction result.[40, 41] The activity increases slowly with the increasing reduction temperatures. The complete CO conversion at room temperature was observed when the catalyst was reduced at 500 and 600 ^oC.

Starting with the Pt-Co/SiO_2 and Au-Co/SiO_2 catalysts reduced at 600 ^oC, oxidation in O_2 was carried out at 100, 200, 300 and 400 ^oC, respectively, and CO oxidation reactions were carried out in between (Figure 8). The activity of the Pt-Co/SiO_2 catalyst strongly depends on the oxidation treatments, which decreases quickly with the increasing oxidation temperatures. In contrast, for the Au-Co/SiO_2 catalyst the influence of the oxidation treatments on the activity is less obvious, and there is a very slight change in the light-off curve of CO oxidation with oxidation up to 400 ^oC. For the CO oxidation under the stoichiometric CO and O_2 condition, the activity of the Pt-Co/SiO_2 and Au-Co/SiO_2 catalysts increases with reduction temperature although the activities are much lower than those for the CO oxidation in excess O_2. Moreover, the oxidation treatments deteriorate the activities of CO oxidation, especially for the reduced Pt-Co/SiO_2 catalysts (Figure S3).

Discussion

Co (CoO_x)-NM interaction during the redox treatments

We have shown that most of CoO_x species in the Pt-Co/SiO_2 sample can be reduced when exposed to H_2 atmosphere within 100 ^oC. This result is also consistent with the finding from Zheng et al, in which they showed that CoO_x species on Pt NPs can be reduced even at 38 ^oC.[42] We have deposited 0.5 monolayer (ML) CoO_x on a Pt(111) surface, and exposed the CoO_x/Pt(111) surface to 1 bar H_2 at room temperature in a high-pressure cell. After the treatment, the cell was evacuated to ultrahigh vacuum (UHV), and the sample was transfer to another UHV chamber for XPS measurements.[43] The recorded XPS Co 2p spectra displayed that the Pt-supported CoO_x overlayer has been fully reduced to Co under the low temperature reduction condition (Figure 9). It has been previously shown that reduction of pure Co oxides supported on SiO_2 starts above 300 ^oC.[44, 45] Obviously, the presence of Pt NPs in the Pt-Co/SiO_2 sample facilitates the reduction of Co oxides at much low temperatures. It is suggested that H_2 molecules dissociate into H atoms on Pt surface at room temperature and these atomic H species can spill over to CoO_x structures nearby enabling them to be reduced at low temperature.[46] After reduction at high temperature, Co tends to diffuse inward and Pt atoms segregate to the surface to release the strain energies arising from the mismatch between Pt (1.39 Å) and Co (1.25 Å).[18, 28, 30, 42,47]

For the Au-Co/SiO_2 catalyst, the reduction of CoO_x proceeds slowly with the reduction treatment, and Co atoms are difficult to diffuse into Au NPs even after reduction at 600 ^oC. Au surface is inert to H_2 dissociation at low temperatures,[48] and thus the promotion effect of Au on the reduction of CoO_x is not significant compared to that of Pt.[49] This can be further confirmed by the study in a 0.5 ML CoO_x/Au(111) surface, in which the surface Co oxide keeps unchanged when treated in 1 bar H_2 at room temperature (Figure 9). Reduction at high temperature did not result in the inward diffusion of Co atoms in Au-Co NPs. Au and Co is immiscible in a wide range of temperature and the heat of mixing between Au and Co is about 7 kJ/mol via an endothermic process.[31, 50] Moreover, as a result of the much stronger interaction of H_2 with Co than that with Au, Co prefers to stay outside of Au NPs.[48, 49] Thus, alloy phase can not form during the high temperature reduction processes.[51, 52]

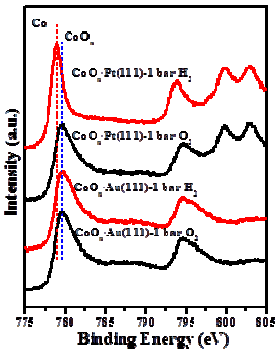

Figure 9. XPS Co 2p spectra from 0.5 ML CoO_x deposited on Pt(111) and Au(111) surfaces treated in 1 bar O_2 and 1 bar H_2 at room temperature, consequently.

Due to the alloy effect of Co with Pt, the oxidation of Co species necessitates the phase segregation of Co from PtCo alloy NPs. The oxidation-driven surface segregation of Co atoms in Pt NPs is thermally activated, and surface CoO_x structures form gradually on Pt NP surfaces with the oxidation at elevated temperatures. XPS and XANES data indicate that the resulting Co oxide structure is CoO. It is the interaction between Pt and CoO_x that prevents the over-oxidation of the metallic Co into Co^{3+} and helps the formation of wetted CoO overlayers.[30, 42, 53]

In the reduced Au-Co/SiO_2 samples, most of Co atoms are outside of Au NPs. As a result, the Co atoms can be easily oxidized in O_2 even at room temperature. Oxidation at higher temperatures should not change the surface structure too much.[31] Even though the Au NPs exert small effect on the Co oxidation, the formed oxide is also CoO, different with the oxidation of Co NPs supported on carbon black.[18] The structural changes of Au-Co/SiO_2 and Pt-Co/SiO_2 systems upon various redox treatments are shown in Figure 10.

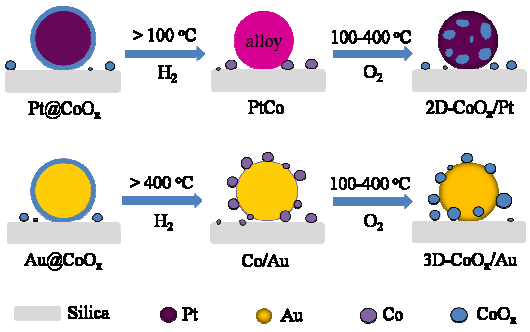

Figure 10. Schematics showing the variation of the surface architecture of Pt-Co/SiO_2 (A) and Au-Co/SiO_2 (B) samples with redox treatments.

Active sites of Pt-Co/SiO_2 and Au-Co/SiO_2 catalysts for CO oxidation

Pure Pt and Au NPs as well as Co species supported on SiO_2 exhibit low activity towards CO oxidation (Figure S4). However, these NM catalysts become highly active through decoration with CoO_x species

combined with appropriate treatments. It seems that the synergistic effect between NM and CoO_x species plays a critical role in the reaction. In our previous works, we have show that the peripheries of FeO nanoislands supported on Pt surfaces contain coordinatively unsaturated ferrous (CUF) sites, which are highly active for the activation of O_2.[26] Later on, a general strategy has been developed to confine coordinatively unsaturated (CUS) TM cations on NM surfaces by constructing oxide-on-metal inverse catalysts and making use of the strong interaction between TM oxide (TMO) and NM. The resulting CUS sites at the edges of the TMO nanostructure grown on NMs are highly active for catalytic oxidation reactions.[23]

For traditional metal-on-oxide catalysts, it has been shown that NM catalysts supported on reducible oxides such as TiO_2 and CeO_2 are more active than those supported on inert oxides such as SiO_2 and Al_2O_3.[54] The strong metal-support interaction between NMs and reducible oxides helps to stabilize smaller NM NPs and, more importantly, to produce active sites at the interfaces between NM NPs and oxide supports.[55, 56] Density functional theory calculations also show that O_2 can be more easily activated at the interface sites between NM and reducible oxides.[57, 58]

The results present in this work confirm that the intimate contact between the NM and Co components is essential for the high CO oxidation activity. Thus, it can be inferred that the reactions mainly occur at the interfaces between the two components. For the Pt-Co/SiO_2 sample, the intimate contact between the Co and Pt components can be achieved with the low temperature reduction treatments. XRD, XANES and XPS characterizations of the catalysts show that all Co species are reduced to the metallic state at 100 ^oC and only a small part of the Co atoms are alloyed with Pt. In oxidative atmosphere, the surface Co species form highly dispersed surface oxide structures, creating high density of interface sites between surface CoO_x structure and Pt support. As shown in Figure 7A, these catalysts present the high activity. The reduction at a high temperature, e.g. 600 ^oC, however, drives the inward diffusion of most Co atoms, forming Pt_3Co alloy nanostructures. In such a case, the number of interface sites between CoO_x surface structure and Pt decreases, lowering the reaction activity. In contrast, high temperature above 500 ^oC is needed to activate the Au-Co/SiO_2 catalysts. For one aspect, the complete reduction of CoO_x species occurs at high temperatures. On the other hand, interaction between Co and Au can be significant only upon reduction at high temperatures. The high temperature reduction treatment helps to increase the density of interface sites between surface CoO_x structure and Au support. Accordingly, the activity of the Au-Co/SiO_2 catalyst increases with the reduction temperature (Figure 7B).

Oxidation treatments on the reduced Pt-Co/SiO_2 sample lead to the surface segregation of alloyed Co atoms and aggregation of surface CoO_x structures. Due to the strong interaction between CoO_x and Pt, the segregated Co atoms tend to form wetted CoO layers on Pt NPs, which can decrease the CoO-Pt interface sites, particularly under high temperature oxidation condition. The structural characterizations show that Co in the reduced Au-Co/SiO_2 catalyst is almost oxidized when exposed to O_2 at room temperature and further oxidation treatment at higher temperatures would not changed the structure of the Au-Co/SiO_2 catalyst too much. The much stronger dependence of the CoO-Pt interfacial structure on the oxidation treatment than the CoO-Au system results in the stronger influence of the oxidation treatment on the activity of the Pt-Co/SiO_2 catalyst than the Au-Co/SiO_2 catalyst.

Conclusion

On the basis of structural characterization and CO oxidation test over the Pt-Co/SiO_2 and Au-Co/SiO_2 catalysts, we made the following conclusions:

1) CoO_x species in the Pt-Co/SiO_2 catalyst can be reduced within 100 ^oC, which is facilitated by the presence of Pt. The Co atoms start to diffuse inside of Pt NPs at relatively low reduction temperatures and form Pt_3Co alloy structures after high temperature reduction treatment.

2) The full reduction of CoO_x in the Au-Co/SiO_2 catalyst necessitates reduction above 400 ^oC, in which Au plays a minor role. With reduction treatments up to 600 ^oC, no strong alloy reaction occurs between Au and Co.

3) Oxidation of Co in the reduced Pt-Co/SiO_2 catalyst takes place gradually due to the slow outward diffusion of alloyed Co atoms, while most of Co in the reduced Au-Co/SiO_2 catalyst has been oxidized upon exposure to O_2 at room temperature since the Co atoms are mostly located at the sample surfaces and get oxidized quickly.

4) The maximum activity was observed over the Pt-Co/SiO_2 catalyst reduced at relatively low temperatures (between 100 and 300 ^oC). For the Au-Co/SiO_2 catalyst, the highest activity was obtained after the reduction at 600 ^oC. The oxidation treatments have much stronger influence on the activity of the Pt-Co/SiO_2 catalyst than the Au-Co/SiO_2 catalyst.

5) In both systems, the CoO-on-NM surface structures are active for the CO oxidation reaction. Treatments to form high density of interface sites between surface CoO structure and NM support can enhance the reactivity.

Acknowledgements

This work was financially supported by the National Natural Science Foundation of China (No. 21222305, No. 11079005, and No. 20923001), and Ministry of Science and Technology of China (No. 2011CBA00503, and No. 2013CB933100).

Notes and references

[a] State Key Laboratory of Catalysis, Dalian Institute of Chemical Physics, Chinese Academy of Sciences, Dalian 116023, China. [b] Department of Electrical Engineering, East China Normal University, Shanghai, 200241, China. E-mail: qfu@dicp.ac.cn (Qiang Fu). Fax: (+86)-411-84694447.

1. A. Y. Khodakov, W. Chu and P. Fongarland, *Chem Rev*, 2007, **107**, 1692.
2. A. Barbier, *J Catal*, 2001, **200**, 106.
3. E. Iglesia, S. L. Soled and R. A. Fiato, *J Catal*, 1992, **137**, 212.
4. G. L. Bezemer, J. H. Bitter, H. P. C. E. Kuipers, H. Oosterbeek, J. E. Holewijn, X. D. Xu, F. Kapteijn, A. J. van Dillen and K. P. de Jong, *J Am Chem Soc*, 2006, **128**, 3956.
5. A. M. Saib, D. J. Moodley, I. M. Ciobîcă, M. M. Hauman, B. H. Sigwebela, C. J. Weststrate, J. W. Niemantsverdriet and J. van de Loosdrecht, *Catal Today*, 2010, **154**, 271.
6. G. Jacobs, T. K. Das, P. M. Patterson, J. Li, L. Sanchez and B. H. Davis, *Appl Catal A-Gen*, 2003, **247**, 335.
7. L. Guczi, D. Bazin, I. Kovacs, L. Borko, Z. Schay, J. Lynch, P. Parent, C. Lafon, G. Stefler, Z. Koppany and I. Sajo, *Top Catal*, 2002, **20**, 129.
8. K. Jalama, N. J. Coville, D. Hildebrandt, D. Glasser, L. L. Jewell, J. A. Anderson, S. Taylor, D. Enache and G. J. Hutchings, *Top Catal*, 2007, **44**, 129.
9. D. Schanke, S. Vada, E. A. Blekkan, A. M. Hilmen, A. Hoff and A. Holmen, *J Catal*, 1995, **156**, 85.
10. H. Wang, W. Zhou, J.-X. Liu, R. Si, G. Sun, M.-Q. Zhong, H.-Y. Su, H.-B. Zhao, J. A. Rodriguez, S. J. Pennycook, J.-C. Idrobo, W.-X. Li, Y. Kou and D. Ma, *J Am Chem Soc*, 2013, **135**, 4149.
11. L. F. Liotta, H. Wu, G. Pantaleo and A. M. Venezia, *Catal Sci Technol*, 2013, **3**, 3085.

12. C.-J. Jia, M. Schwickardi, C. Weidenthaler, W. Schmidt, S. Korhonen, B. M. Weckhuysen and F. Schuth, *J Am Chem Soc*, 2011, **133**, 11279.
13. J. Jansson, A. E. C. Palmqvist, E. Fridell, M. Skoglundh, L. Österlund, P. Thormählen and V. Langer, *J Catal*, 2002, **211**, 387.
14. Y. Y. Liang, Y. G. Li, H. L. Wang, J. G. Zhou, J. Wang, T. Regier and H. J. Dai, *Nature Mater*, 2011, **10**, 780.
15. E. B. Castro, C. A. Gervasi and J. R. Vilche, *J Appl Electrochem*, 1998, **28**, 835.
16. F. Jiao and H. Frei, *Angew Chem Int Ed*, 2009, **48**, 1841.
17. M. Haruta, S. Tsubota, T. Kobayashi, H. Kageyama, M. J. Genet and B. Delmon, *J Catal*, 1993, **144**, 175.
18. H. Xu, Q. Fu, X. Guo and X. Bao, *ChemCatChem*, 2012, **4**, 1645.
19. C. Wang, B. D. Li, H. Q. Lin and Y. Z. Yuan, *J Power Sources*, 2012, **202**, 200.
20. B. S. Yeo and A. T. Bell, *J Am Chem Soc*, 2011, **133**, 5587.
21. W. Yu, M. D. Porosoff and J. G. Chen, *Chem Rev*, 2012, **112**, 5780.
22. Z. Wei, J. Sun, Y. Li, A. K. Datye and Y. Wang, *Chem Soc Rev*, 2012, **41**, 7994.
23. Q. Fu, F. Yang and X. H. Bao, *Acc Chem Res*, 2013, **46**, 1692.
24. H.-L. Jiang and Q. Xu, *J Mater Chem*, 2011, **21**, 13705.
25. A. Wang, X. Y. Liu, C.-Y. Mou and T. Zhang, *J Catal*, 2013, **308**, 258.
26. Q. Fu, W.-X. Li, Y. Yao, H. Liu, H.-Y. Su, D. Ma, X.-K. Gu, L. Chen, Z. Wang, H. Zhang, B. Wang and X. Bao, *Science*, 2010, **328**, 1141.
27. F. Bao, J.-F. Li, B. Ren, J.-L. Yao, R.-A. Gu and Z.-Q. Tian, *J Phys Chem C*, 2008, **112**, 345.
28. R. Mu, Q. Fu, H. Liu, D. Tan, R. Zhai and X. Bao, *Appl Surf Sci*, 2009, **255**, 7296.
29. C. A. Menning and J. G. Chen, *J Power Sources*, 2010, **195**, 3140.
30. V. Papaefthimiou, T. Dintzer, V. R. Dupuis, A. Tamion, F. Tournus, D. Teschner, M. Havecker, A. Knop-Gericke, R. Schlogl and S. Zafeiratos, *J Phys Chem Lett*, 2011, **2**, 900.
31. H. Okamoto. and T. B. Massalski, *Bulletin of Alloy Phase Diagrams*, 1985, **6**, 449.
32. J. H. Choy, H. Jung and J. B. Yoon, *J Synchrotron Radiat*, 2001, **8**, 599.
33. M. Voß, D. Borgmann and G. Wedler, *J Catal*, 2002, **212**, 10.
34. K. Qian, W. Huang, Z. Jiang and H. Sun, *J Catal*, 2007, **248**, 137.
35. R. Riva, H. Miessner, R. Vitali and G. Del Piero, *Appl Catal A-Gen*, 2000, **196**, 111.
36. R. Mu, X. Guo, Q. Fu and X. Bao, *J Phys Chem C*, 2011, **115**, 20590.
37. H. Xu, Q. Fu, Y. Yao and X. Bao, *Energy Environ. Sci.*, 2012, **5**, 6313.
38. R. Mu, Q. Fu, H. Xu, H. Zhang, Y. Huang, Z. Jiang, S. Zhang, D. Tan and X. Bao, *J Am Chem Soc*, 2011, **133**, 1978.
39. T. Ma, Q. Fu, H.-Y. Su, H.-Y. Liu, Y. Cui, Z. Wang, R.-T. Mu, W.-X. Li and X.-H. Bao, *ChemPhysChem*, 2009, **10**, 1013.
40. X. J. Xu, Q. Fu, X. G. Guo and X. H. Bao, *ACS Catal*, 2013, **3**, 1810.
41. K. Qian, W. Huang, J. Fang, S. Lv, B. He, Z. Jiang and S. Wei, *J Catal*, 2008, **255**, 269.
42. F. Zheng, S. Alayoglu, J. Guo, V. Pushkarev, Y. Li, P.-A. Glans, J.-l. Chen and G. Somorjai, *Nano Lett*, 2011, **11**, 847.
43. Q. Fu, Y. Yao, X. Guo, M. Wei, Y. Ning, H. Liu, F. Yang, Z. Liu and X. Bao, *Phys Chem Chem Phys*, 2013, **15**, 14708.
44. G. Jacobs, Y. Ji, B. H. Davis, D. Cronauer, A. J. Kropf and C. L. Marshall, *Appl Catal A-Gen*, 2007, **333**, 177.
45. N. Osakoo, R. Henkel, S. Loiha, F. Roessner and J. Wittayakun, *Appl Catal A-Gen*, 2013, **464-465**, 269.
46. H. Karaca, O. V. Safonova, S. Chambrey, P. Fongarland, P. Roussel, A. Griboval-Constant, M. Lacroix and A. Y. Khodakov, *J Catal*, 2011, **277**, 14.
47. J. S. Tsay and C. S. Shern, *J Appl Phys*, 1996, **80**, 3777.
48. J. Greeley and M. Mavrikakis, *Nature Mater*, 2004, **3**, 810.
49. S. Zhou, H. Yin, V. Schwartz, Z. Wu, D. Mullins, B. Eichhorn, S. H. Overbury and S. Dai, *ChemPhysChem*, 2008, **9**, 2475.
50. A. Takeuchi and A. Inoue, *Mater Trans*, 2005, **46**, 2817.
51. A. M. Molenbroek, J. K. Norskov and B. S. Clausen, *J Phys Chem B*, 2001, **105**, 5450.
52. R. P. Galhenage, S. C. Ammal, H. Yan, A. S. Duke, S. A. Tenney, A. Heyden and D. A. Chen, *J Phys Chem C*, 2012, **116**, 24616.
53. M. De Santis, A. Buchsbaum, P. Varga and M. Schmid, *Phys Rev B*, 2011, **84**, 125430.
54. M. M. Schubert, S. Hackenberg, A. C. van Veen, M. Muhler, V. Plzak and R. J. Behm, *J Catal*, 2001, **197**, 113.
55. I. X. Green, W. Tang, M. Neurock and J. T. Yates, *Science*, 2011, **333**, 736.
56. H. Y. Kim, H. M. Lee and G. Henkelman, *J Am Chem Soc*, 2012, **134**, 1560.
57. Z.-P. Liu, X.-Q. Gong, J. Kohanoff, C. Sanchez and P. Hu, *Phys Rev Lett*, 2003, **91**, 266102.
58. D. P. Sun, X. K. Gu, R. H. Ouyang, H. Y. Su, Q. Fu, X. H. Bao and W. X. Li, *J Phys Chem C*, 2012, **116**, 7491.